JACS
JOURNAL OF THE AMERICAN CHEMICAL SOCIETY
Article
pubs.acs.org/JACS

Redox-Induced Ion Pairing of Anionic Surfactants with Ferrocene-Terminated Self-Assembled Monolayers: Faradaic Electrochemistry and Surfactant Aggregation at the Monolayer/Liquid Interface

Eric R. Dionne, Tania Sultana, Lana L. Norman, Violeta Toader,[†] and Antonella Badia*

Department of Chemistry, Centre for Self-Assembled Chemical Structures of the Fonds de recherche du Québec-Nature et technologies, Université de Montréal, C.P 6128 succursale Centre-ville, Montréal, Quebec H3C 3J7, Canada

Supporting Information

ABSTRACT: Oxidoreduction of self-assembled monolayers (SAMs) of ferrocenyldodecanethiolate on gold in aqueous solutions of surface-active sodium *n*-alkyl sulfates (NaC_nSO_4) of 6, 8, 10, and 12 carbons is investigated by cyclic voltammetry and surface plasmon resonance. The effects of surfactant micellization and alkyl chain length on the redox response of the surface-tethered ferrocenes are examined. The SAM redox electrochemistry is sensitive to the surfactant aggregation state in solution. The nonideal behavior of the sodium alkyl sulfates at concentrations above the critical micelle concentration leads to a non-Nernstian variation of the SAM redox potential with concentration. The presence of micelles in solution results in decreased anodic-to-cathodic peak separations and anodic peak full widths at half-maximum. A longer alkyl chain length results in an increased ability of the alkyl sulfate anion to ion pair with the SAM-bound ferrocenium, resulting in oxidation of the ferrocene at lower potential. A comparison of the SAM redox potential at a fixed surfactant concentration of ideal behavior suggests a 4.5×10^4 difference in the ion-pairing abilities of the shorter-chain $C_6SO_4^-$ and longer-chain $C_{12}SO_4^-$. One-half of the available SAM-bound ferrocenes are oxidized in the NaC_nSO_4 electrolyte. Surfactant anions adsorb and assemble onto the SAM surface by specific ion-pairing interactions between the sulfate headgroups and oxidized ferrocenium species, forming an interdigitated monolayer in which the surfactant anions alternate between a heads-down and heads-up orientation with respect to the SAM. The work presented points to applications of ferrocenylalkanethiolate SAMs as anion-selective membranes, probes of micelle formation, and surfaces for the electrochemically switchable assembly of organosulfates.

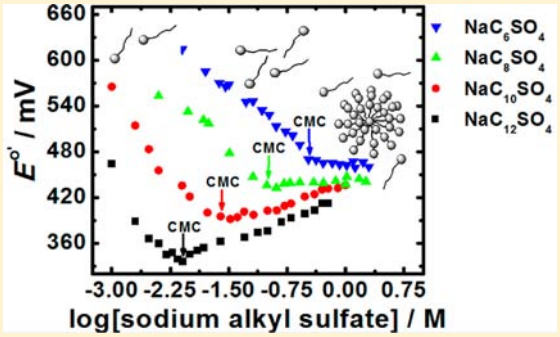

INTRODUCTION

This article reports the interfacial electrochemistry of self-assembled monolayers (SAMs) of ferrocenyldodecanethiolate on gold electrodes in aqueous solutions of sodium *n*-alkyl sulfates, anionic surfactants that form micelles in water above the critical micelle concentration. We show that the SAM redox response is exquisitely sensitive to the surfactant aggregation state in solution and that the surfactant anions adsorb and assemble onto the SAM surface by specific ion-pairing interactions between the sulfate headgroups and the oxidized ferrocenium species. By varying the length of the hydrocarbon chain from 6 to 12 carbons, the ability of the alkyl sulfate to pair with the SAM-bound ferrocenium could be varied by a factor of 4.5×10^4. The surface-confined redox reaction provides a reversible means of directing the interfacial adsorption and desorption of the surface-active anions. The molecular organization of the surfactant at the ferrocenium SAM/liquid interface differs from the aggregate structures formed by electrostatic adsorption to charged surfaces. The work presented points to electron-transfer-induced ion pairing with surface-tethered redox moieties as an effective strategy for assembling amphiphilic molecules at solid/liquid interfaces via an electrical stimulus.

SAMs of ferrocenylalkanethiolate, ca. 1−3 nm thick, chemisorbed to gold electrode surfaces were initially designed in the early 1990s for fundamental studies of long-range interfacial electron transfer across a well-defined and chemically tailorable organic layer.[1−4] Numerous reports have focused on the electrochemical properties and interfacial electron-transfer dynamics of clustered and isolated ferrocenes in single-component and mixed binary SAMs.[5−16] The ferrocene/ferrocenium (Fc/Fc^+) couple exhibits relatively straightforward electrochemistry, and SAM-bound ferrocenes can be reversibly interrogated by potential-induced Faradaic reaction. Oxidation of the SAM-bound Fc to Fc^+ proceeds via coupled electron-transfer and ion-pairing reactions

$$Fc \rightleftharpoons Fc^+ + e^-$$

$$Fc^+ + X^- \rightleftharpoons Fc^+X^- \quad (1)$$

Received: August 16, 2013
Published: October 16, 2013

   dx.doi.org/10.1021/ja408512q | J. Am. Chem. Soc. 2013, 135, 17457−17468

The Fc^+X^- (1:1 ion pair) formation constant K is defined as

$$K = \Gamma_{Fc^+X^-}/\Gamma_{Fc^+}a_{X^-} \quad (2)$$

where Γ_{Fc^+} and $\Gamma_{Fc^+X^-}$ are the surface concentrations of Fc^+ and ion-paired Fc^+ and a_{X^-} is the activity of the anion X^- in solution.[7,11] Formation of a specific contact ion pair between the electrogenerated Fc^+ and X^- stabilizes the surface-tethered oxidized cation.[14] Hydrophobic anions, such as PF_6^-, ClO_4^-, and BF_4^-, pair more effectively with the poorly solvated Fc^+ than hydrophilic ones, such as Cl^-, SO_4^{2-}, and F^-.[7,11,14,17] The nature of the anion strongly affects the redox response in cyclic voltammetry (i.e., number of surface ferrocenes oxidized, half-wave potential, anodic peak current, formal width at half-maximum of the anodic peak, anodic-to-cathodic peak separation) and stability of the ferrocene-terminated SAM upon repeated potential cycling in aqueous solution.[7,11,14,18]

The apparent redox potential of the ferrocenylalkanethiolate SAM ($E^{o'}_{SAM}$) is given by the Nernst equation for the electron-transfer and ion-pairing reactions

$$E^{o'}_{SAM} = E^{o}_{SAM} + 2.303\frac{RT}{F}\log\frac{(\Gamma_{Fc^+})_{total}}{\Gamma_{Fc}K} - 2.303\frac{RT}{F}\log a_{X^-} \quad (3)$$

where E^{o}_{SAM} is the standard redox potential of the SAM-bound ferrocenes and $(\Gamma_{Fc^+})_{total} = \Gamma_{Fc^+} + \Gamma_{Fc^+X^-}$.[7,11] Molar concentrations ($[X^-]$) are typically used in place of activities (a_{X^-}) in eqs 2 and 3 in studies of the ion pairing of monovalent inorganic anions with ferrocene-terminated SAMs.[7,8,11,19,20] Equation 3 shows that the SAM redox potential depends on the Fc^+X^- ion-pair formation constant K and the anion activity in solution a_{X^-}. No such dependence of the redox potential on the nature of the anion and concentration is observed for ferrocene derivatives in solution.[9] This contrasting ferrocene surface versus solution behavior is attributable to the necessity to neutralize the excess positive charge that is generated at the SAM/electrolyte solution interface upon oxidation of Fc to Fc^+ and stabilize Fc^+ in the typically nonpolar and sterically crowded SAM environment.[9,10,20]

The work described herein extends previous investigations of electrolyte anion effects on the oxidation of ferrocenylalkanethiolate SAMs to surface-active organic anions that consist of a hydrophobic hydrocarbon tail and a hydrophilic anionic headgroup. The idea is to combine the tendency of anionic surfactants to aggregate at solid/liquid interfaces[21] with the preference of SAM-bound ferroceniums to pair with lipophilic anions.[7,11,14,17] Sodium *n*-alkyl sulfates (NaC_nSO_4) were chosen as prototypes for study because these are commonly used surfactants in consumer and industrial applications. We have previously shown the reversible oxidation and reduction of ferrocenylalkanethiolate SAMs in aqueous solutions of sodium dodecyl sulfate.[22] By choosing a homologous series of 6, 8, 10, and 12 carbon chains for study, the overall hydrophobic character of the surfactant is varied while keeping the ion-pairing sulfate headgroup fixed.

Sodium alkyl sulfates are strong electrolytes. These salts are soluble in water at temperatures greater than the Krafft temperature and are completely dissociated at low bulk concentrations. When the surfactant concentration exceeds a critical value, known as the critical micelle concentration (cmc), the alkyl sulfate monomers spontaneously aggregate to form spherical or spherocylindrical micelles, depending on the concentration, solution ionic strength, and nature of the counterion.[23,24] The cmc decreases with increasing chain length from 420 mM for sodium hexyl sulfate (NaC_6SO_4) to 8.1 mM for sodium dodecyl sulfate ($NaC_{12}SO_4$) in water, and the micellar aggregation number increases from 17 to 64, respectively.[23,24] The activity or effective concentration of the alkyl sulfate anion above the cmc is governed by the chemical equilibria between the free surfactant anion monomers, counterions (Na^+), and micelles.[23,25] The redox potential of the ferrocene SAM allows us to track changes in the alkyl sulfate monomer activity in solution.

The Faradaic electrochemistry of SAMs of ferrocenyldodecanethiolate on gold ($FcC_{12}SAu$) is investigated by cyclic voltammetry in aqueous solutions of NaC_6SO_4, NaC_8SO_4, $NaC_{10}SO_4$, and $NaC_{12}SO_4$ at concentrations below, at, and above the cmc. Adsorption of surfactant anions to the oxidized SAM is monitored in real time and quantified by surface plasmon resonance.

MATERIALS AND METHODS

Chemicals. 12-Ferrocenyl-1-dodecanethiol ($FcC_{12}SH$) was synthesized using procedures adapted from the literature.[26,27] Friedel–Crafts acylation of ferrocene with 12-bromododecanoyl chloride in dry dichloromethane at 0 °C gave 12-bromododecanoyl ferrocene that was subsequently hydrogenated at room temperature using a mixture of triethyl silane (4 equiv) and titanium(IV) chloride (1 equiv) in dry dichloromethane. The 12-bromodecyl ferrocene obtained in this manner was reacted with thiourea in absolute ethanol to give 12-ferrocenyldodecyl isothiuronium bromide in quantitative yield. 12-Ferrocenyl-1-dodecanethiol was obtained by hydrolysis of the isothiuronium intermediate under basic conditions. The final product was purified by flash chromatography over silica gel by elution with a 9:1 (v/v) mixture of hexanes and dichloromethane. Fractions with $R_f = 0.37$ were collected. The purity of the product (0.2366 g, 37% yield) was verified by ^{1}H NMR spectroscopy (400 MHz, $CDCl_3$, δ (ppm)): 4.12 (s, 5H, H_{Fc}), 4.09 (s, 2H, H_{Fc} ortho to ~CH_2–CH_2~), 4.07 (s, 2H, H_{Fc} meta to ~CH_2–CH_2~), 2.52 (q, 2H, ~CH_2–CH_2–SH), 2.29 (t, 2H, Fc–CH_2~), 1.61 (quintet, 2H, ~CH_2–CH_2–SH), 1.5–1.26 (m, 18H, ~$(CH_2)_9$–$(CH_2)_2$–SH~), 1.33 (t, 1H, –*SH*).

The following reagents were purchased and used without further purification: sodium perchlorate (99+%, Acros Organics), perchloric acid (70%, American Chemicals Ltd.), sodium *n*-hexyl sulfate (NaC_6SO_4, 99%, Research Plus), sodium *n*-octyl sulfate (NaC_8SO_4, ≥99%, Fluka or 99%, Alfa Aesar), sodium *n*-decyl sulfate ($NaC_{10}SO_4$, 99%, Alfa Aesar or Research Plus), and sodium *n*-dodecyl sulfate ($NaC_{12}SO_4$, 99%, Sigma-Aldrich or Alfa Aesar). Sodium methyl sulfate (NaC_1SO_4, Sigma-Aldrich) was recrystallized once from hot anhydrous ethanol before use.

All aqueous electrolyte solutions were prepared with ultrapure water (18.2 MΩ·cm) obtained by purification of distilled water with a Milli-Q Gradient system (Millipore, Bedford, MA). $NaClO_4$/$HClO_4$ solutions were purged with N_2 gas for at least 30 min prior to electrochemical experiments to minimize oxygen levels. Surfactant solutions were prepared immediately before use to prevent hydrolysis with ultrapure water that had been purged for at least 30 min with N_2 gas.

Preparation of $FcC_{12}SAu$ SAMs. B270 glass slides (Esco Products Inc.) were cleaned by immersion in piranha solution (3:1 v/v H_2SO_4/30% H_2O_2) for 5 min at room temperature. B270 substrates were rinsed thoroughly with ultrapure water, sonicated thrice in water to completely remove traces of sulfuric acid, and dried under a stream of nitrogen gas. Clean glass slides were coated on one side by a 2 nm layer of Ti (99.99%, Alfa Aesar) followed by a 50 nm layer of Au (99.99%, Kitco Metals, Inc.) using a VE-90 thermal evaporator (Thermionics Vacuum Products). Metal thickness and deposition rate were monitored using a calibrated quartz crystal microbalance. Deposition of metal was initiated once the pressure inside the evaporation chamber reached ~5×10^{-7} Torr. Ttitanium and gold layers were evaporated at rates of 0.01 and 0.02 nm s^{-1}, respectively. The pressure at the end of the gold evaporation was ~1.8×10^{-6} Torr.

Polycrystalline gold bead electrodes were formed by bonding a 2–3 mm diameter gold granule (99.99%, Kitco Metals, Inc.) to a 0.5 mm

diameter gold wire (99.99%, Alfa Aesar) with a butane torch. The gold bead at the end of the gold wire was immersed in aqua regia (3:1 HCl/HNO_3) to remove surface impurities and then remelted. The gold bead was dipped twice for 5 min in piranha solution (3:1 v/v H_2SO_4/30% H_2O_2), rinsed thoroughly with ultrapure water, and dried under a stream of nitrogen gas.

Gold-coated B270 slides and gold beads were immersed for a minimum of 12 h in a 0.2 mM solution of $FcC_{12}SH$ in absolute ethanol. The incubation process was carried out at room temperature, and incubation vials were kept in the dark. Prior to use, the $FcC_{12}SAu$ SAM-modified substrate was removed from the $FcC_{12}SH$ incubation solution, rinsed copiously with absolute ethanol followed by ultrapure water, and dried with nitrogen.

Cyclic Voltammetry. All cyclic voltammograms were acquired in a custom-built, one-compartment three-electrode Teflon cell. The $FcC_{12}SAu$-modified substrate served as the working electrode. A platinum wire (99.99%, Sigma-Aldrich) and Ag/AgCl electrode (3 M NaCl, BASi) were used as the counter and reference electrodes. The Ag/AgCl electrode was inserted in a double-junction chamber (BASi) filled with electrolyte solution to minimize leaching of chloride ions into the electrochemical cell compartment. CVs were acquired at a potential scan rate of 10 mV s^{-1} using either an Epsilon potentiostat (BASi) or a SI 1287 Electrochemical Interface (Solartron). Experiments were performed at a temperature of 21 ± 1 °C.

The surface concentration of electrogenerated ferrocenium (Γ_{Fc^+}) was determined using eq 4

$$\Gamma_{Fc^+} = Q_{Fc^+}/nFA \tag{4}$$

where Q_{Fc^+} is the charge associated with ferrocene oxidation determined by integration of the anodic peak(s) corrected for the background charging current, n represents the number of electrons involved in the electrochemical process (n = 1 for the oxidation of ferrocene to ferrocenium), F is the Faraday constant (96 485 C mol^{-1}), and A is the area of the $FcC_{12}SAu$ surface exposed to the electrolyte solution.[28] Mathematical integration and deconvolution of the anodic peaks were done using Microcal Origin version 6.0 software.

Electrochemical Surface Plasmon Resonance. Measurements were carried out in the Kretschmann-type attenuated ATR configuration with a computer-controlled SR7000 single-channel instrument (Reichert Inc.). The instrument uses stationary optics, a sapphire prism, a divergent fan-shaped beam from a light source of finite spectral bandwidth (λ = 780 ± 10 nm), and a 3696-pixel linear CCD array to simultaneously measure the reflected light intensity over a range of angles of incidence (Θ of 48−66°). The temperature at the gold/liquid interface is controlled to within ±0.015 °C of the set temperature between 10 and 90 °C by a Peltier device.

A custom-built electrochemical cell fitted with reference (Ag/AgCl, 3 M NaCl electrode inserted in a double junction chamber) and counter (Pt wire) electrodes was mounted onto the gold-coated surface of the B270 glass slide (working electrode) in optical contact with the prism. The pixel position of minimum reflected light intensity was recorded under stationary conditions as the applied potential was cycled between 0 and +600 mV (vs Ag/AgCl) at a rate of 5 mV s^{-1}. Experiments were carried out at 25 °C.

Shifts in the pixel position of minimum reflected light intensity were converted to resonance angle changes ($\Delta\Theta_{min}$) using the pixel-to-angle relation of 1 pixel = 0.0506° determined by calibration of the SR7000 instrument using binary mixtures of ethylene glycol and water of different refractive index.[29] Adsorbed layer thicknesses (d) were determined using the variation of Θ_{min} with the effective layer thickness of pure $C_{10}SO_4^-$ or $C_{12}SO_4^-$ ($\partial\Theta_{min}/\partial d$) calculated with the modeling section of the eSPIRe software program (Resonant Probes GmbH), a hemicylindrical prism geometry, λ of 780 nm, and the Fresnel multilayer model given in Table 1 (i.e., $\partial\Theta_{min}/\partial d$ = 0.0396° nm^{-1} for $C_{10}SO_4^-$ and 0.0405° nm^{-1} for $C_{12}SO_4^-$)

$$d = \Delta\Theta_{min}\left(\frac{\partial\Theta}{\partial d}\right)^{-1} \tag{5}$$

The surface concentration or coverage (Γ) of adsorbed alkyl sulfate is obtained from the effective layer thickness as follows

$$\Gamma = d\Delta n\left(\frac{\partial n}{\partial c}\right)^{-1} \tag{6}$$

where Δn is the difference in the refractive indices of the adsorbate layer ($n_{adsorbate}$ = 1.449, see footnote h of Table 1) and pure solvent (n_{water} = 1.3281 at 780 nm and 25 °C),[30] and $\partial n/\partial c$ is the incremental change in refractive index with increasing surfactant concentration.[31] Values of $\partial n/\partial c$ of 2.98 × 10^{-5} and 3.40(±0.05) × 10^{-5} mM^{-1} were determined for $NaC_{10}SO_4$ and $NaC_{12}SO_4$, respectively, by critical angle reflectance measurements at 780 nm and 25 °C.[32] Unlike d and $n_{adsorbate}$, Γ does not assume the presence of a uniform adsorbate layer.[33]

Table 1. Fresnel Layer Model and Optical Parameters

layer	medium	n	k	d /nm
1	sapphire prism	1.76074[a]	0	∞[b]
2	Ti adhesion layer	2.7683[c]	3.3065[c]	2.0[d]
3	Au layer	0.181[e]	4.856[e]	50.0[d]
4	$-S(CH_2)_{12}Fc^+$ SAM	1.464[f]	0	2.02[g]
5	adsorbed surfactant	1.449[h]	0	varied from 0 to 5 nm
6	33.2 mM $NaC_{10}SO_{4(aq)}$ or 8.1 mM $NaC_{12}SO_{4(aq)}$	1.3291[i] or 1.3284[i]	0	∞[b]

[a]Refractive index at 780 nm and 24 °C from ref 58. [b]Signifies of infinite thickness. [c]Complex refractive index at 780 nm from ref 59. [d]Mass thickness indicated by the quartz crystal microbalance at the end of metal evaporation. [e]Value determined by spectroscopic ellipsometry at 780 nm. [f]Refractive index from ref 60. [g]Thickness determined by spectroscopic ellipsometry in air for the SAM in the reduced state. [h]Value found by measuring the refractive index of aqueous solutions containing 0−25 mass % of $NaC_{12}SO_4$ and extrapolating the linear relation to 100 mass %. [i]Solution refractive index determined by critical angle reflectance measurements at 780 nm and 25 °C.

RESULTS AND DISCUSSION

Alkyl Sulfate versus Perchlorate Anion Electrochemistry. Figure 1A shows the cyclic voltammogram (CV) typically recorded for $FcC_{12}SAu$ SAMs formed on polycrystalline gold thin films in an aqueous solution containing 0.100 M $NaClO_4$/0.010 M $HClO_4$ (pH 2.1). The $NaClO_4$ solution was acidified with $HClO_4$ to protect the oxidized ferrocenes from nucleophilic attack.[34] ClO_4^- is the electrolyte anion commonly employed for this type of electroactive SAM because it forms a strong (contact) interfacial ion pair with the ferrocenium that stabilizes the electrogenerated cation.[7−11,14] The CV resembles some of those already published for single-component ferrocene-terminated SAMs.[5,8,16,35,36] The SAM-bound ferrocenes exhibit a nonideal "reversible" electrochemical behavior.[10] Ideal or near-ideal electrochemistry of SAM-bound ferrocenes, characterized by single symmetrical redox peaks with full widths at half-maximum of 90.6 mV and no anodic-to-cathodic peak potential separation,[28] is generally only observed for binary SAMs in which the surface mole fraction of ferrocene is less than about 0.25 and single isolated ferrocenylalkanethiolates are surrounded by inert alkanethiolates.[5,10,13] There are two pairs of redox peaks that do not change over multiple consecutive scans. The apparent redox potential $E^{\circ\prime}$, taken as the half-wave potential or average of the anodic (oxidation) and cathodic (reduction) peak potentials, of the first pair of peaks is 305 ± 11 mV, and that of the second pair is 417 ± 4 mV (n = 9 electrodes). The anodic-to-cathodic peak separation (ΔE_p) is 19 ± 5 mV for the first pair of

dx.doi.org/10.1021/ja408512q | J. Am. Chem. Soc. 2013, 135, 17457−17468

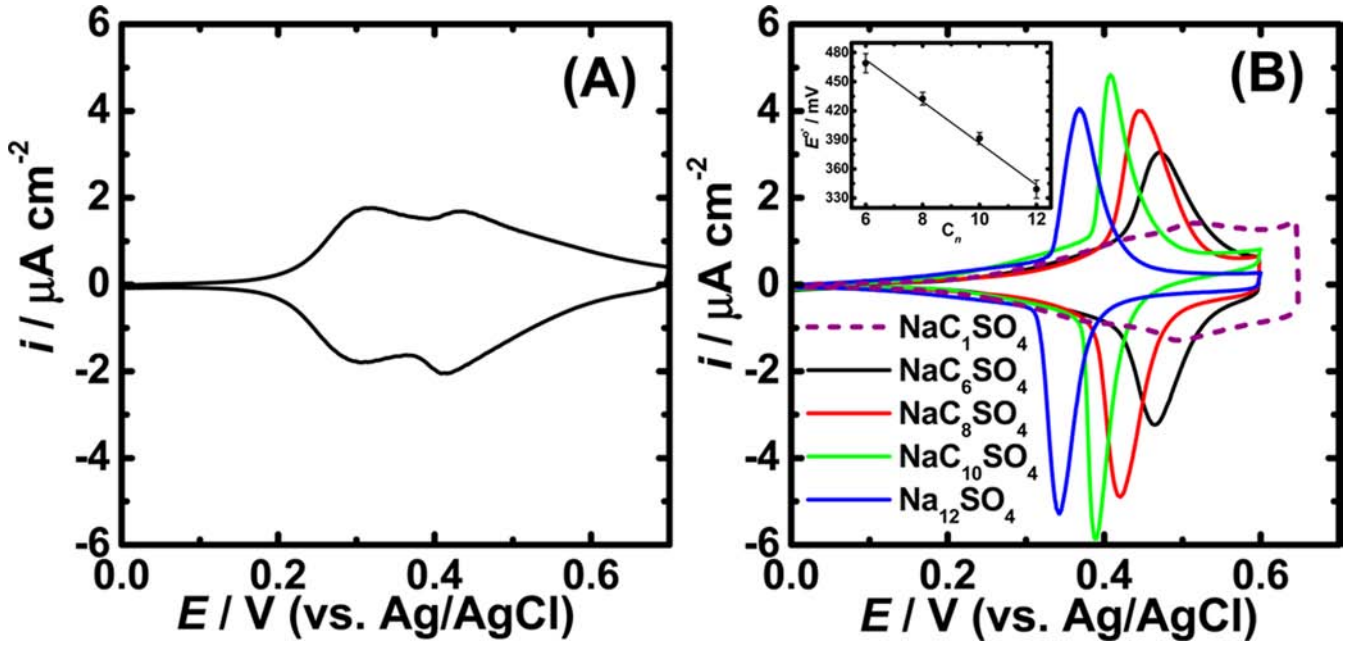

Figure 1. CVs of $FcC_{12}SAu$ SAMs on gold thin film electrodes recorded in different aqueous electrolyte solutions at a scan rate of 10 mV s^{-1}. (A) 0.100 M $NaClO_4$/0.010 M $HClO_4$ (pH 2.1). (B) Sodium *n*-alkyl sulfates at the cmc: 420 mM sodium hexyl sulfate (NaC_6SO_4), 130 mM sodium octyl sulfate (NaC_8SO_4), 33.2 mM sodium decyl sulfate ($NaC_{10}SO_4$), and 8.1 mM sodium dodecyl sulfate ($NaC_{12}SO_4$). CV in 100 mM sodium methyl sulfate (NaC_1SO_4) is also shown. (Inset) Plot of the $FcC_{12}SAu$ SAM redox potential $E^{\circ\prime}$ measured at the cmc versus the number of carbons C_n in the hydrocarbon chain of the surfactant anion. Linear regression ($r = -0.9955$) gives a slope of −21.5 mV C_n^{-1}. Data points and error bars are the average and standard deviation of at least 3 different $FcC_{12}SAu$ SAMs.

peaks and 13 ± 4 mV for the second pair. Both anodic peaks, peak I at 315 ± 12 mV and peak II at 423 ± 5 mV, exhibit the linear dependence of the peak current on potential scan rate expected for a surface-confined redox reaction (Figure S1, Supporting Information).[28] The total anodic peak area yields a charge associated with ferrocene oxidation (Q_{Fc^+}) of 44 ± 3 μC cm^{-2} and a corresponding electrogenerated ferrocenium surface concentration of 4.6 (±0.3) × 10^{-10} mol cm^{-2}, which is close to the theoretical maximum surface coverage of ferrocene of 4.5 × 10^{-10} mol cm^{-2}.[5]

The presence of two pairs of voltammetric peaks is attributable to electrochemically distinct ferrocene populations of differing intermolecular interactions caused by the heterogeneity in the surface density and molecular ordering of the ferrocenylalkanethiolates across the SAM.[15,16] Electrostatic repulsion between the ferrocenium cations and steric constraints/crowding render oxidation of ferrocenes found inside close-packed domains less favorable (higher anodic potential) than those located at domain boundaries and monolayer defect sites (lower potential).[6,9,13,15,37] A mathematical deconvolution of the anodic scan using Gaussian−Lorentzian fitting[15,16,18] (see Figure S2, Supporting Information) yields the relative ferrocene populations and full width at half-maximum (ΔE_{fwhm}) of each anodic peak: peak I 27 ± 6% ferrocene, ΔE_{fwhm} = 98 ± 14 mV; peak II 73 ± 6% ferrocene, ΔE_{fwhm} = 161 ± 17 mV. ΔE_{fwhm} is a qualitative indicator of the presence and nature of the interactions between the surface-bound redox centers. As already mentioned, a ΔE_{fwhm} of 90.6 mV is expected for the ideal case where all of the ferrocenes have equivalent environments and there are minimal interactions between them (Langmuir isotherm).[28] The significantly larger ΔE_{fwhm} of the peak II ferrocene population reflects the predominance of repulsive interactions between the ferroceniums, consistent with assignment of the higher potential redox peak to closely packed ferrocenes.[16,28]

The Faradaic electrochemistry of $FcC_{12}SAu$ SAMs in solutions of NaC_nSO_4 homologues of C_n = 6, 8, 10, and 12 in ultrapure water is markedly different from that in $NaClO_4/HClO_4$ electrolyte. Shown in Figure 1B are the CVs recorded at bulk surfactant concentrations equal to the cmc. All CVs were run at ambient temperature (21 ± 1 °C), which is well above the Krafft temperature of the longest-chain $NaC_{12}SO_4$ (16 °C).[38] No background electrolyte or acid was used to ensure that the alkyl sulfate anions are the only ion-pairing species in solution. Single anodic and cathodic peaks with tailing on the negative potential side are observed instead of the two sets of redox peaks recorded in $NaClO_4/HClO_4$. The $FcC_{12}SAu$ SAMs are stable in the sodium alkyl sulfate solutions and do not show significant variations in the peak current, position, or shape over at least six consecutive oxidoreduction cycles performed at a scan rate of 10 mV s^{-1} (Figure S3, Supporting Information). Furthermore, the near-linear variation of the peak current with the potential scan rate confirms that the anodic peak is due to oxidation of the surface-bound ferrocenes.[22] The CVs acquired for $FcC_{12}SAu$ SAMs formed on evaporated gold films and annealed gold beads (data not shown) exhibit the same characteristics.

The well-defined and sharp voltammetric peaks indicate that the alkyl sulfate homologues ion pair with and stabilize the electrogenerated ferroceniums. By contrast, the electrochemical oxidation and reduction of the $FcC_{12}SAu$ SAM in the presence of the more hydrophilic and non-surface-active $CH_3SO_4^-$ yield broad voltammetric waves with low peak currents (Figure 1B, dashed line). Anions with poor ion-pairing abilities, such as F^-, SO_4^{2-}, and Cl^-, yield CVs with broad asymmetric redox peaks shifted to more anodic peak potentials and lower peak currents that irreversibly decrease on repeated cycling due to nucleophilic attack and demetallization of the ferroceniums.[14,18,34] This is clearly not the case for the 6−12 carbon *n*-alkyl sulfates. The ΔE_{fwhm} values of the anodic peaks (45−60 mV) are significantly

dx.doi.org/10.1021/ja408512q | J. Am. Chem. Soc. 2013, 135, 17457−17468

less than 90.6 mV (ideal case), reflecting the existence of attractive interactions between the ferroceniums,[28] in striking contrast to oxidation of the same $FcC_{12}SAu$ SAMs in the presence of ClO_4^-, which is dominated by repulsive intermolecular interactions and yields $\Delta E_{fwhm} > 90.6$ mV.

Integration of the voltammetric anodic peaks of the CVs acquired in $NaC_6SO_{4(aq)}$, $NaC_8SO_{4(aq)}$, $NaC_{10}SO_{4(aq)}$, and $NaC_{12}SO_{4(aq)}$ (n = 352 electrodes) yields a Q_{Fc^+} of 23 ± 5 μC cm^{-2} (see Figures S4 and S5, Supporting Information, for examples of Q_{Fc^+} determination), which corresponds to about 52% of the charge density obtained for the same SAMs with perchlorate anions (i.e., 44 ± 3 μC cm^{-2}). This decreased charge density is not due to the diminished ion-pairing ability of the alkyl sulfates with respect to the perchlorate anions but can be related to the physical crowding of ferrocene moieties in the SAM and the steric constraints associated with oxidation and ion pairing (coupled reactions) of all the available ferrocenes with the alkyl sulfate anions. This hypothesis is suggested by a previous study in which ferrocenium charge densities were determined for oxidation of mixed $FcC_{11}SAu/HOC_{11}SAu$ SAMs consisting of different ferrocene surface mole fractions (χ_{Fc}) in $NaC_{12}SO_{4(aq)}$.[22] The ferrocenes are diluted out by non-electroactive hydroxyalkanethiolates in the mixed SAMs so that the average surface density of ferrocenes and the extent of ferrocene clustering/crowding decrease as χ_{Fc} decreases.[15] A nearly 1:1 linear correlation between Q_{Fc^+} and χ_{Fc} is observed up to χ_{Fc} of 0.5 (i.e., implying that essentially all of the available ferrocenes are oxidized). At $\chi_{Fc} > 0.5$, Q_{Fc^+} remains quasi-constant at a value of ~28 μC cm^{-2}.[22]

Although the $C_6SO_4^-$ (monomer) solution concentration is 52 times greater than that of $C_{12}SO_4^-$ at their respective cmcs, the apparent redox potential of the $FcC_{12}SAu$ SAM in $NaC_6SO_{4(aq)}$ ($E^{\circ\prime}$ = 470 mV) is 130 mV more positive than the redox potential in $NaC_{12}SO_{4(aq)}$ ($E^{\circ\prime}$ = 340 mV). In fact, the redox potential measured at the cmc shifts linearly to more negative values with increasing alkyl chain length (Figure 1B, inset). The linear relation between the measured redox potentials and the number of carbons in the hydrocarbon chain is surprising given that these were measured at different sodium alkyl sulfate concentrations and the Nernst equation predicts a dependence of the redox potential on the anion activity (see eq 3). In fact, the same dependence of $E^{\circ\prime}$ with C_n, i.e., slope of −22 ± 3 mV C_n^{-1}, is found at NaC_nSO_4 concentrations equal to 0.25 × cmc, 0.5 × cmc, and 2 × cmc (Figure S6, Supporting Information). The linear relationship between $E^{\circ\prime}$ and C_n must reflect a dependence of the $C_nSO_4^-$ ion-pairing ability on the chain length.

If the standard redox potential of the SAM-bound ferrocenes E°_{SAM} was known, the ion-pairing ability (i.e., ion-pair formation constant K) of each alkyl sulfate anion could be quantitatively determined using eq 3.[11] Since E°_{SAM} is not known, we calculate the relative ion-pairing abilities of the longer-chain $C_{12}SO_4^-$, $C_{10}SO_4^-$, and $C_8SO_4^-$ versus the shorter-chain $C_6SO_4^-$ (reference anion) using eq 7[11]

$$\frac{K_{C_nSO_4^-}}{K_{C_6SO_4^-}} = \frac{a_{C_6SO_4^-}}{a_{C_nSO_4^-}} \exp\left[\frac{F(E^{o'}{}_{C_6SO_4^-} - E^{o'}{}_{C_nSO_4^-})}{RT}\right] \quad (7)$$

and the redox potentials measured at a fixed sodium alkyl sulfate concentration of 8.0 mM, concentration equal to the cmc of the longest-chain $NaC_{12}SO_4$ used in this study, and at which all surfactant solutions behave ideally (i.e., $a_{C_6SO_4^-}$, $a_{C_8SO_4^-}$, $a_{C_{10}SO_4^-}$, and $a_{C_{12}SO_4^-}$ are equal to [NaC_nSO_4] of 8.0 mM).[25] $K_{C_nSO_4^-}/K_{C_6SO_4^-}$ of 44 800, 1065, and 21 are calculated for $C_{12}SO_4^-$, $C_{10}SO_4^-$, and $C_8SO_4^-$, respectively, confirming the influence of the hydrocarbon chain length on the ability of the alkyl sulfate anions to pair with and stabilize the SAM-bound ferroceniums. As the length of the alkyl chain increases, the overall hydrophobic character of the surfactant increases and can better satisfy the preference of the ferrocenium to pair with more hydrophobic anions. There is also a greater tendency of the alkyl sulfate to adsorb and aggregate (via dispersion forces) at charged solid/liquid interfaces as the chain length increases.[21,39] The (4.5 × 10^4)-fold higher ion-pairing ability imparted by the additional six methylenes in the hydrocarbon chain of $C_{12}SO_4^-$ versus $C_6SO_4^-$ is remarkable given that a comparison of the redox potentials of different types of ferrocene-terminated SAMs measured in aqueous solutions of sodium salts of inorganic anions using eq 7 shows differences ranging from 47.5 to 243 in the ion-pairing abilities of the more hydrophobic (weakly hydrated) ClO_4^-, which forms contact ion pairs with the SAM-bound ferroceniums, and the hydrophilic (hydrated) Cl^-, which has one of the poorest ion-pairing abilities.[9,11,14] We obtain $K_{ClO_4^-}/K_{Cl^-}$ of 116 with the $FcC_{12}SAu$ SAM. With differences in ion-pairing abilities ≥ 10^4, one may envisage the preferential pairing of the more hydrophobic alkyl sulfate anion with the SAM-bound ferroceniums from a mixed binary solution and the broader possibility of using ferrocene-terminated SAMs as anion-selective membranes to detect organosulfates[40] based on differences in ion-pair formation constants.

Effect of the Sodium Alkyl Sulfate Concentration on the Faradaic Electrochemistry. The dependence of $E^{\circ\prime}$, ΔE_p, and ΔE_{fwhm} on the surfactant concentration is examined in more detail. CVs acquired at surfactant concentrations ranging from 0.125 × cmc to 8 × cmc are shown in Figure 2A. Q_{Fc^+} remains quasi-constant (within the data scatter) at an average value of 23 μC cm^{-2} (Figure 2B). Approximately the same number of SAM-bound ferrocenes are oxidized as a function of the surfactant concentration. The positions of the anodic and cathodic peaks shift to lower potential as the surfactant concentration is decreased from above the cmc to the cmc of each sodium alkyl sulfate and then shifts back to higher potential as the concentration is further decreased below the cmc. This behavior is in marked contrast to the unidirectional shift to higher potential of the anodic and cathodic peaks with decreasing electrolyte concentration observed for oxidation and reduction of $FcC_{12}SAu$ SAMs in $NaClO_4$-containing solution (Figure S7A, Supporting Information, and refs 8 and 11). CVs also show a significant broadening of the voltammetric peaks, decrease in peak currents, as well as peak splitting in the case of the shorter-chain $C_6SO_4^-$ and $C_8SO_4^-$ at surfactant concentrations below the cmc. Figure 3 presents plots of the $E^{\circ\prime}$, ΔE_p, and ΔE_{fwhm} values extracted from the CVs as a function of the common logarithm of the sodium alkyl sulfate molar concentration/cmc ratio, where log ([NaC_nSO_4]/cmc) = 0 at the cmc. All plots show breaks around the cmc.

First, we consider the variation of the measured redox potential $E^{\circ\prime}$ of the $FcC_{12}SAu$ SAM with the logarithm of the sodium alkyl sulfate concentration (Figure 3A). For the longer-chain $NaC_{10}SO_4$ and $NaC_{12}SO_4$, $E^{\circ\prime}$ is at its minimum value at the cmc and increases at surfactant concentrations above the cmc and below the cmc, giving "V-shaped" plots (Figure 3A) instead of a Nernstian-type linear relation.[7,8,11,20] In the case of the shorter-chain NaC_6SO_4 and NaC_8SO_4, $E^{\circ\prime}$ is nearly constant at concentrations above the cmc and increases quasi-linearly with

dx.doi.org/10.1021/ja408512q | J. Am. Chem. Soc. 2013, 135, 17457−17468

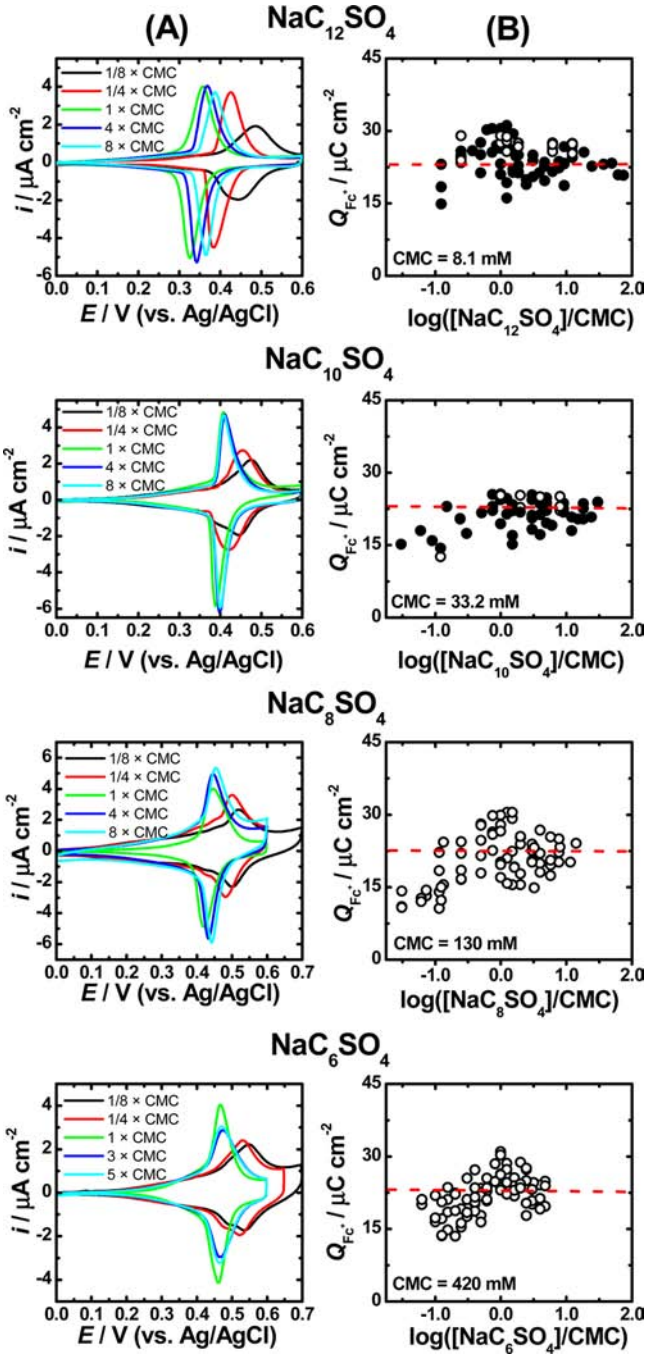

Figure 2. Electrochemistry of $FcC_{12}SAu$ SAMs in $NaC_6SO_{4(aq)}$, $NaC_8SO_{4(aq)}$, $NaC_{10}SO_{4(aq)}$, and $NaC_{12}SO_{4(aq)}$. (A) CVs as a function of the bulk NaC_nSO_4 concentration expressed as a multiple of the cmc. (B) Ferrocenium charge density Q_{Fc}^+ versus the logarithm of the NaC_nSO_4 molar concentration/cmc ratio, where $\log([NaC_nSO_4]/cmc) = 0$ at the cmc. Open and filled data points indicate values from $FcC_{12}SAu$ SAMs formed on gold thin film and gold bead electrodes, respectively. Dashed line indicates average Q_{Fc}^+ of 23 μC cm^{-2}. Since the cmc's of the NaC_nSO_4 homologues span a wide range, $[NaC_nSO_4]$ is normalized with respect to the cmc to facilitate visual location of the cmc. $\log([NaC_nSO_4]/cmc) = 0$ at the cmc.

decreasing concentration below the cmc. The dependence of $E^{o\prime}_{SAM}$ on the electrolyte anion concentration is given by eq 3.[7,11] If $E^{o\prime}_{SAM}$ is measured when the surface mole fractions of Fc and Fc^+ are equal (i.e., at the half-wave potential), eq 3 reduces to

$$E^{o\prime}_{SAM} = E^{o}_{SAM} - 2.303\frac{RT}{F}\log K - 2.303\frac{RT}{F}\log a_{X^-} \quad (8)$$

As indicated by eq 8, the redox potential of the $FcC_{12}SAu$ SAM is sensitive to the electrolyte anion activity, analogous to the potential measured by indicator electrodes.[41] A linear relationship with a slope of approximately −59 mV is nonetheless observed between $E^{o\prime}$ and the logarithm of the molar concentration of $NaClO_4$ (or $HClO_4$) (Figure S7B, Supporting Information, and slope of −58 ± 6 mV for refs 7, 8, 11, 19, and 20) because of the nearly 1:1 correspondence between $\log[NaClO_4]$ and $\log a_{ClO_4^-}$ in the concentration range from 0.001 to 0.5 M (Figure S7C, Supporting Information), ClO_4^- being a relatively small monovalent anion (hydrated ion radius of 0.35 nm)[42] and $NaClO_4$ (or $HClO_4$) being a strong 1,1-electrolyte.

For ionic surfactants that exist in solution as either monomers (below the cmc) or a mixture of monomers and micellar aggregates (above the cmc) there are important differences between the activity of the surfactant monomer ion and molar concentration of the salt above the cmc,[23,25,43,44] as shown from the data of Evans et al.[25] for NaC_8SO_4, $NaC_{10}SO_4$, and $NaC_{12}SO_4$ in water presented in Figure 4A. The near-Nernstian responses (slopes of 54−59 mV decade^{-1}) observed by potentiometry using surfactant-ion-specific electrodes at bulk concentrations below the cmc indicate that sodium alkyl sulfates behave as typical 1,1-electrolytes below the cmc.[25,43,44] There is no significant premicellar aggregation of the surfactant up to the cmc so that the activity of the alkyl sulfate anion (monomer) in solution is equal to the concentration of added salt. Deviations from ideal behavior are observed at sodium alkyl sulfate concentrations > cmc.[25,43,44] The alkyl sulfate anion activity is at its maximum around the cmc and decreases above the cmc due to aggregation of the dissociated anions into micelles. The difference between the activity of the alkyl sulfate ion and molar concentration of sodium alkyl sulfate in solution increases with increasing hydrocarbon chain length (Figure 4A).[25]

Using the redox potential measured in 1 M $NaClO_{4(aq)}$ for single isolated ferrocenes in a binary $FcC_{12}SAu/C_{11}SAu$ SAM of ferrocene surface mole fraction of 0.18 ($E^{o\prime}$ = 180 mV) as an *estimate* of E^{o}_{SAM} and $K_{C_nSO_4^-}/K_{C_6SO_4^-}$ in place of K, relative apparent redox potentials ($E^{o\prime}_{SAM\ rel}$) are calculated using eq 8 from the activities reported by Evans et al.[25] for $C_8SO_4^-$, $C_{10}SO_4^-$, and $C_{12}SO_4^-$ and graphed against log ($[NaC_nSO_4]$/cmc) in Figure 4B. The plots resemble those obtained for the measured redox potential $E^{o\prime}$ of the $FcC_{12}SAu$ SAM (Figure 4B, inset). The $E^{o\prime}_{SAM\ rel}$−log ($[NaC_nSO_4]$/cmc) plots exhibit minima around the cmc of each surfactant (i.e., because the anion activity is at its maximum near log ($[NaC_nSO_4]$/cmc) = 0 and the inverse relation between $E^{o\prime}_{SAM}$ and a_{X^-} in eq 8). The $E^{o\prime}_{SAM\ rel}$ value at the minimum is chain length dependent and follows the same order, i.e., $E^{o\prime}_{SAM\ rel}$ (NaC_8SO_4) > $E^{o\prime}_{SAM\ rel}$ ($NaC_{10}SO_4$) > $E^{o\prime}_{SAM\ rel}$($NaC_{12}SO_4$), as the redox potentials associated with the minima or breaks that occur around the cmc in the $E^{o\prime}$−log($[NaC_nSO_4]$/cmc) plots of the $FcC_{12}SAu$ SAM (Figures 3A and 4B, inset), establishing that the SAM redox potential at the cmc is dictated by the ion-pair formation constant (or ion-pairing ability of the $C_nSO_4^-$). Moreover, plots of the $E^{o\prime}_{SAM\ rel}$ calculated at surfactant concentrations equal to 0.25 × cmc, 0.5 × cmc, cmc, and 2 × cmc versus C_n are linear ($r > 0.999$) with a slope of −29 ± 1 mV C_n^{-1} (Figure S8, Supporting Information). This value is comparable to the slope of −22 ± 3 mV C_n^{-1} of the plots of $E^{o\prime}$ of the $FcC_{12}SAu$ SAM versus C_n at the same concentration

dx.doi.org/10.1021/ja408512q | J. Am. Chem. Soc. 2013, 135, 17457−17468

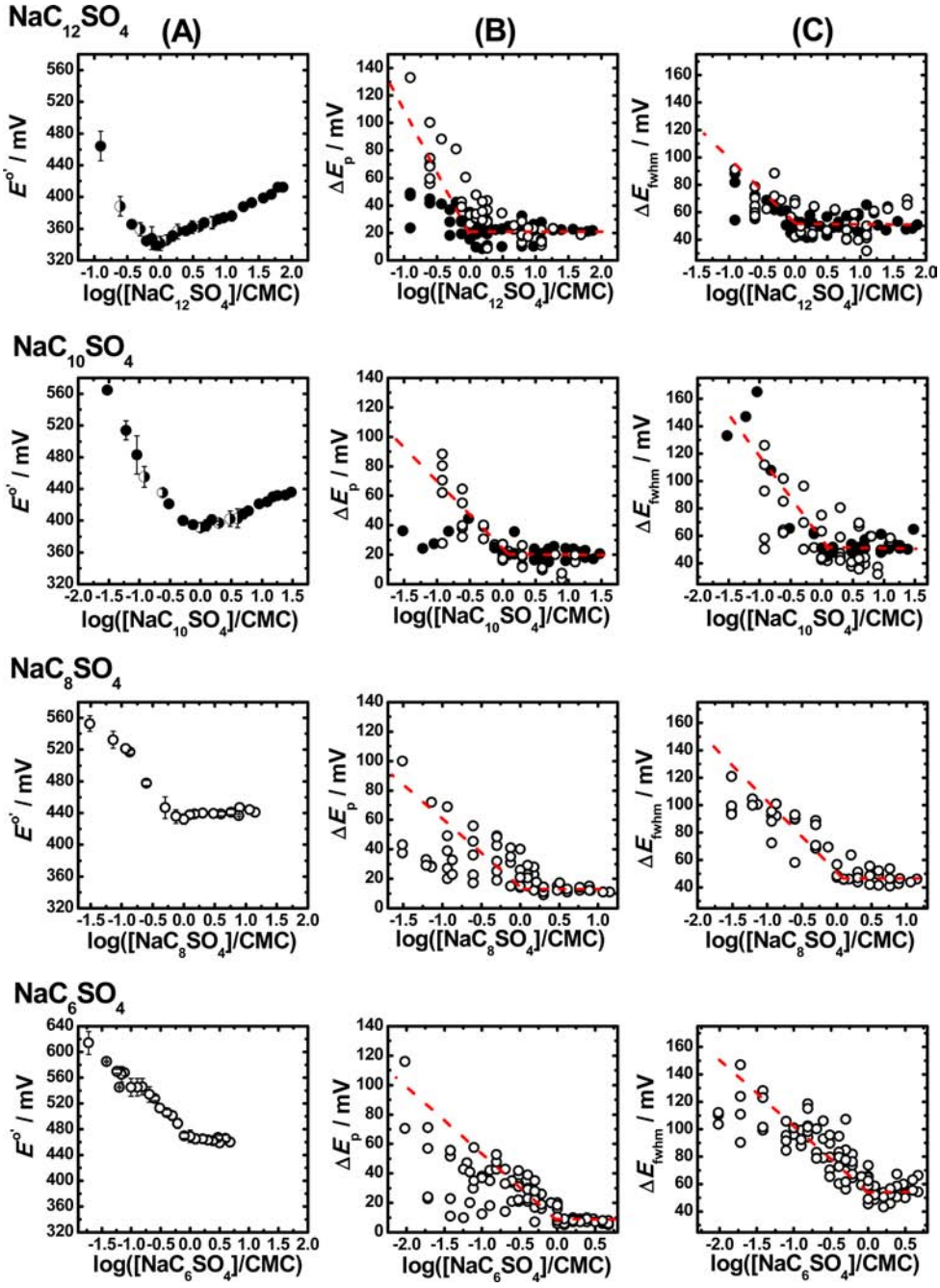

Figure 3. CV data for $FcC_{12}SAu$ SAMs versus $\log([NaC_nSO_4]/cmc)$. (A) Measured SAM redox potential $E^{\circ\prime}$. (B) Anodic-to-cathodic peak separation ΔE_p. (C) Formal width at half-maximum ΔE_{fwhm} of the anodic peak. Data points and error bars in A are the average and standard deviation of $E^{\circ\prime}$ for at least 3 different SAMs. Open, filled, and half-filled data points indicate values from SAMs formed on gold thin films, gold beads, and average of gold thin film and bead electrodes, respectively. Dashed lines are guides to the eye.

multiples of cmc (Figure S6, Supporting Information). The fact we can reproduce using eq 8 the overall variation of the redox potential measured for the SAM-bound ferrocenes with the NaC_nSO_4 concentration indicates that the non-Nernstian behavior of the SAM redox potential is primarily due to the surfactant anion activity in the bulk solution.

Plots of the calculated $E^{\circ\prime}_{SAM\ rel}$ and measured $E^{\circ\prime}$ versus the logarithm of the *activity* of $C_nSO_4^-$ support this conclusion (Figure 5). These are linear with slopes equal or close to −59 mV. In the case of the $E^{\circ\prime}$−log $a_{C_nSO_4^-}$ plots (Figure 5, inset), the deviations from −59 mV are attributable to liquid junction potentials,[45,46] which are convolved in the measured redox potentials and uncompensated solution resistance (potential drop),[28] especially at low (mM) NaC_nSO_4 concentration, which causes the observed potential at the working electrode to be lower than that indicated by the potentiostat. Both the liquid junction potential and the uncompensated solution resistance vary with electrolyte concentration. No positive feedback IR compensation was applied during the CV measurements, and attempts at measuring the liquid junction potential as a function of the $NaC_{12}SO_4$ concentration using the procedure described in ref 46 did not yield reproducible results.

Now we consider the variation of the redox peak separations and anodic peak widths with the surfactant concentration. Given

dx.doi.org/10.1021/ja408512q | J. Am. Chem. Soc. 2013, 135, 17457−17468

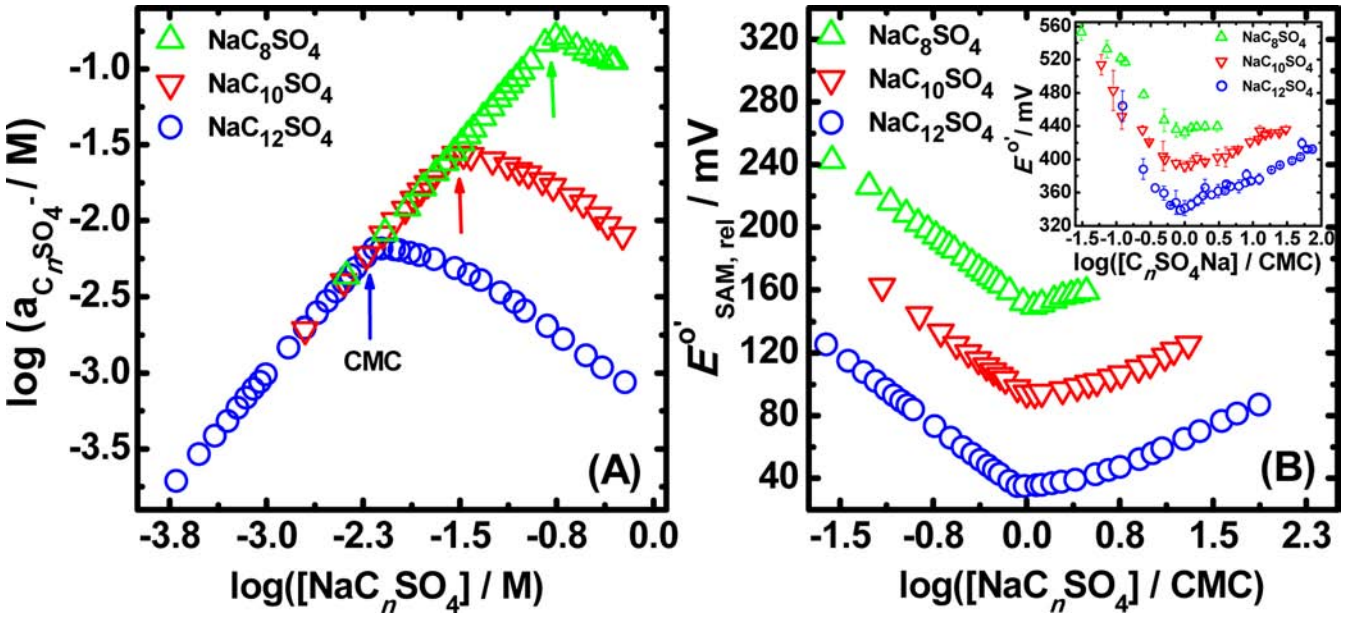

Figure 4. (A) Plots of the logarithm of the $C_nSO_4^-$ (free monomer anion) activity versus the logarithm of the NaC_nSO_4 molar concentration. $C_8SO_4^-$, $C_{10}SO_4^-$, and $C_{12}SO_4^-$ activities are from the work of Evans et al.[25] (B) Plots of the relative apparent redox potentials $E^{o\prime}_{SAM\ rel}$ calculated using eq 8 from $K_{C_nSO_4^-}/K_{C_6SO_4^-}$ and the activities reported by Evans et al.[25] for $C_8SO_4^-$, $C_{10}SO_4^-$, and $C_{12}SO_4^-$ versus log ([NaC_nSO_4]/cmc). (Inset) Plots of the measured $FcC_{12}SAu$ SAM redox potential $E^{o\prime}$ versus log ([NaC_nSO_4]/cmc) for NaC_8SO_4, $NaC_{10}SO_4$, and $NaC_{12}SO_4$.

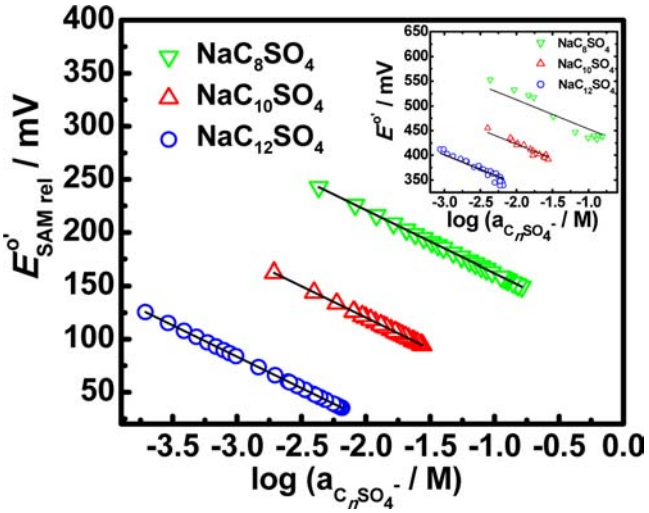

Figure 5. Plots of the relative apparent redox potentials $E^{o\prime}_{SAM\ rel}$ calculated using eq 8 from $K_{C_nSO_4^-}/K_{C_6SO_4^-}$ and activities reported by Evans et al.[25] for $C_8SO_4^-$, $C_{10}SO_4^-$, and $C_{12}SO_4^-$ versus log $a_{C_nSO_4^-}$. (Inset) Plots of the measured $FcC_{12}SAu$ SAM redox potential $E^{o\prime}$ versus log $a_{C_nSO_4^-}$, where the alkyl sulfate anion activities $a_{C_nSO_4^-}$ were interpolated from the $a_{C_nSO_4^-}$ molar concentration of NaC_nSO_4 data tabulated by Evans et al.[25] and shown in Figure 4A. Lines are linear regressions with a fixed slope of −59 mV.

the nonideal behavior of the NaC_nSO_4 solutions in the micelle regime, one might expect broader voltammetric peaks, decreased peak currents, and increased peak separations at surfactant concentrations greater than the cmc. The opposite trend is apparent in the CVs presented in Figure 2A. Redox peaks are significantly broader, peak currents are lower, and peak separations are larger at surfactant concentrations equal to 0.125 × cmc and 0.25 × cmc compared to concentrations of cmc to 8 × cmc, even though the anodic charge density (i.e., area of the anodic peak) remains fairly constant with the NaC_nSO_4 concentration (Figure 2B). Plots of ΔE_p and ΔE_{fwhm} of the anodic peak versus log ([NaC_nSO_4]/cmc) show breaks around the cmc. Although the scatter in the data points is quite large, two regions can be distinguished as indicated by the dashed straight lines drawn in Figure 3B and 3C. At solution concentrations above the cmc (i.e., log ([NaC_nSO_4]/cmc) > 0), ΔE_p and ΔE_{fwhm} do not vary significantly with [NaC_nSO_4]. In this region, ΔE_p increases with chain length from ∼7 mV for NaC_6SO_4 to ∼23 mV for $NaC_{12}SO_4$. ΔE_{fwhm} does not vary much with chain length; average values are between ∼50 ($NaC_{12}SO_4$) and ∼59 mV (NaC_6SO_4). Below the cmc (i.e., log ([NaC_nSO_4]/cmc) < 0), ΔE_p and ΔE_{fwhm} increase as the NaC_nSO_4 concentration decreases.

Unlike the $E^{o\prime}$ values, the variations of ΔE_p and ΔE_{fwhm} with the surfactant concentration cannot be rationalized in terms of the activity of the alkyl sulfate anion in the bulk solution. For example, the data of Evans et al. (Figure 4A) shows that the activity of $C_{12}SO_4^-$ is 2 mM at $NaC_{12}SO_4$ concentrations of 2 (0.25 × cmc) and 150 mM (18.5 × cmc).[25] Similar redox potentials are measured at these two $NaC_{12}SO_4$ concentrations ($E^{o\prime}$ = 388 ± 12 mV at 2 mM and $E^{o\prime}$ = 387 ± 2 mV at 150 mM) because the $C_{12}SO_4^-$ activity is the same, but the CVs do not coincide in their peak current intensities, peak separations, and peak widths.

An increase in ΔE_p and decrease in peak current in cyclic voltammetry are usually associated with an increase in the uncompensated solution resistance as the electrolyte concentration decreases.[28] CVs obtained in $NaClO_4/HClO_4$ solution show changes in ΔE_p and ΔE_{fwhm} at $NaClO_4$ concentrations below ∼10 mM (Figure S9, Supporting Information). Since the sodium alkyl sulfates used in this study have very different cmc's, the amount of uncompensated solution resistance below the cmc is different for each one. For example, in the case of $NaC_6SO_{4(aq)}$, the observed increases in ΔE_p and ΔE_{fwhm} and decrease in peak currents occur over the surfactant concentration range from 26.5

dx.doi.org/10.1021/ja408512q | J. Am. Chem. Soc. 2013, 135, 17457−17468

to 420 mM (i.e., tens to hundreds of millimolar), while for $NaC_{12}SO_{4(aq)}$ the surfactant concentration range is from 1 to 8 mM (i.e., millimolar). If these changes were entirely effects of uncompensated solution resistance, their onset should occur at approximately the same NaC_nSO_4 concentration and not vary with chain length. It appears that the presence of micelles in solution leads to narrower voltammetric peaks, increased peak currents, and reduced peak separations.

Electrochemical Surface Plasmon Resonance. Surface plasmon resonance measurements confirm that the alkyl sulfates bind to the oxidized SAM. The current and resonance angle change ($\Delta\Theta_{min}$) with respect to time for three cyclic voltammetric scans of the $FcC_{12}SAu$ SAM between 0 and +600 mV (vs Ag/AgCl) in 33.2 mM $NaC_{10}SO_{4(aq)}$ are shown in Figure 6A. The resonance angle change tracts the Faradaic current

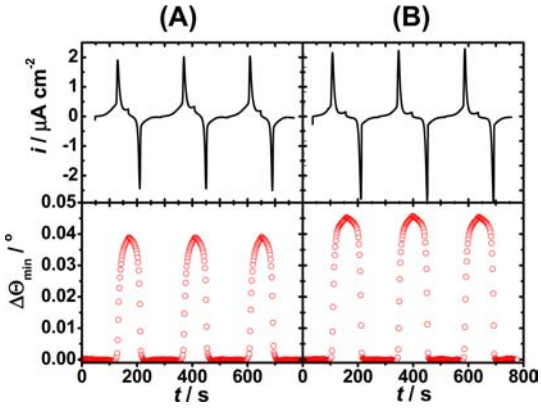

Figure 6. Current i versus time t (top) and corresponding resonance angle change $\Delta\Theta_{min}$ versus time t (bottom) obtained for linear potential cycling of $FcC_{12}SAu$ SAMs between 0 and +600 mV (vs Ag/AgCl) at 5 mV s^{-1} in NaC_nSO_4 at the cmc: (A) 33.2 mM $NaC_{10}SO_{4(aq)}$ and (B) 8.1 mM $NaC_{12}SO_{4(aq)}$.

response in that there is no change in resonance angle prior to generation of a redox current. The resonance angle increases by $0.038 \pm 0.002°$ upon oxidation of the surface-bound ferrocene to ferricinium (anodic segment) and decreases by the same magnitude upon reduction (cathodic segment). The resonance angle changes are fully reversible over multiple oxidation–reduction cycles. Likewise, oxidation of the $FcC_{12}SAu$ SAM in an 8.1 mM aqueous solution of the longer-chain $NaC_{12}SO_4$ yields a $\Delta\Theta_{min}$ of $0.045 \pm 0.003°$ (Figure 6B). Resonance angle changes of the same magnitude are obtained at bulk solution concentrations above the cmc. By comparison, oxidation of the $FcC_{12}SAu$ SAM in 0.100 M $NaClO_4$/0.010 M $HClO_4$ produces a resonance angle shift of $0.020 \pm 0.001°$.[18,29] It is proposed that the steric constraints associated with formation of neighboring, surface-bound $Fc^+ClO_4^-$ pairs requires a collective molecular reorientation which leads to an increase in the SAM thickness of the order of 0.4–0.5 nm.[9,18,29,47] We attribute the larger shifts in resonance angle measured in $NaC_{10}SO_{4(aq)}$ and $NaC_{12}SO_{4(aq)}$ versus $NaClO_4/HClO_{4(aq)}$ to the presence of a layer of bound or adsorbed alkyl sulfate at the oxidized SAM/solution interface.

Effective thicknesses (thicknesses with no water content) of 0.96 ± 0.03 and 1.11 ± 0.04 nm are calculated for the interfacial layers of $C_{10}SO_4^-$ and $C_{12}SO_4^-$, respectively, using the refractive index of pure $NaC_{12}SO_4$ (1.449) and the Fresnel model given in Table 1 of the Methods and Materials section, which supposes that there is no significant oxidation-induced reorganization and thickening of the SAM given that only one-half of the available ferrocenes are oxidized to ferroceniums in the presence of $C_{10}SO_4^-$ or $C_{12}SO_4^-$ anions (i.e., less steric constraints). Adsorbed surfactant concentrations (Γ) of 3.8 ($\pm$0.1) $\times 10^{-10}$ and 3.9 ($\pm$0.3) $\times 10^{-10}$ mol cm^{-2} are determined, respectively, for $C_{10}SO_4^-$ and $C_{12}SO_4^-$ from the effective layer thicknesses using eq 6. We previously obtained an adsorbed $C_{12}SO_4^-$ layer thickness and surface coverage of 1.2 ± 0.1 nm and $4.4(\pm 0.4) \times 10^{-10}$ mol cm^{-2} above the cmc for oxidation of a $FcC_{11}SAu$ SAM.[22] Similar saturation coverages and/or monomolecular layer thicknesses have been reported for adsorption of $NaC_{12}SO_4$ at different interfaces: air/aqueous solution (Gibbs monolayer),[44,48] hydrophobic solid/aqueous solution,[49−51] and electrified single-crystal Au(111)/aqueous solution[52−54] at metal charge densities from −10 to +7 μC cm^{-2} (see Table S1, Supporting Information).

AFM imaging of a hydrophobic $CH_3(CH_2)_{10}SAu$ SAM formed on atomically flat gold on mica[49] and high-resolution STM imaging of an electrified single-crystal Au(111) surface[52] immersed in aqueous solutions of $NaC_{12}SO_4$ unequivocally show that Γ of 3.9–4.0 $\times 10^{-10}$ mol cm^{-2} corresponds to a laterally nanostructured monolayer consisting of hemicylindrical micelle stripes of dodecyl sulfate (Scheme 1A). In the case of adsorption

Scheme 1. Surfactant Anion Adsorbate Structures at the Solid/Aqueous Solution Interface:(A) Hemicylindrical Micelles, (B) Interdigitated Monolayer, and (C) Bilayer

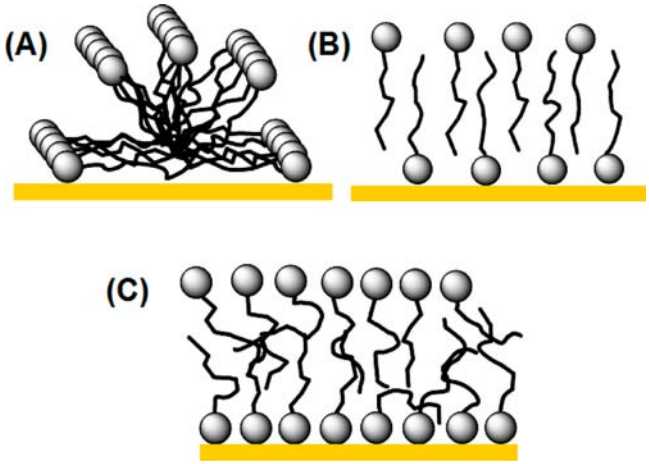

as a continuous monolayer film the more thermodynamically favorable structure at the solid/aqueous solution interface would be an interdigitated configuration in which one-half of the surfactant anions are oriented with their sulfate headgroups toward the SAM ("heads down") and one-half have their headgroups exposed to the aqueous environment ("heads up") (Scheme 1B),[49,53] as opposed to one where all of the surfactant anions have their hydrophobic tails exposed to the aqueous solution. The heads-down surfactant anions would be those ion paired to the ferroceniums.

Are the $C_{10}SO_4^-$ and $C_{12}SO_4^-$ anions adsorbed onto the $Fc^+C_{12}SAu$ SAM as continuous monolayers or hemicylindrical micellar aggregates? SPR reports the total surface concentration of surfactant anions, but both morphologies give total surface concentrations on the order of 4.0×10^{-10} mol cm^{-2}. To answer the question, we must compare the number of surfactant anions that would be paired to the ferroceniums, which are the only ones detected electrochemically, for the cylindrical hemimicelle and interdigitated monolayer configurations, assuming 1:1

dx.doi.org/10.1021/ja408512q | J. Am. Chem. Soc. 2013, 135, 17457−17468

$Fc^+C_nSO_4^-$ stoichiometric pairs, as per ClO_4^-. There are five $C_{12}SO_4^-$ monomers in the unit cell of the 2D lattice of hemicylindrical $C_{12}SO_4^-$ aggregates (Scheme 1A).[52] Only two of the five monomers lie flat with their sulfate headgroups on the solid surface and can therefore potentially ion pair with the $Fc^+C_{12}SAu$ SAM, in a unit cell area of 4.4 nm ×0.50 nm. Such a configuration would yield an electrochemical surface coverage of 1.5×10^{-10} mol cm^{-2} and $Q_{Fc}{}^+$ of 14.5 μC cm^{-2} (i.e., $Q = \Gamma \times F$), which is significantly less than the value of 23 ± 5 μC cm^{-2} obtained experimentally. In the interdigitated monolayer structure, the heads-down surfactant anions are ion paired to ferroceniums generated by oxidation of one-half of the available ferrocenes, giving an electrochemical surface coverage of 2.25×10^{-10} mol cm^{-2} (i.e., calculated by taking one-half of the theoretical maximum surface concentration of ferrocene of 4.5×10^{-10} mol cm^{-2})[5] and $Q_{Fc}{}^+$ of 21.7 μC cm^{-2}, which is comparable to the measured charge density. Since only one out of two available ferrocenes are oxidized, and hence ion paired with an alkyl sulfate and the theoretical area per $FcC_{12}SAu$ is 0.37 nm^2,[5] while the cross-sectional areas of the sulfate headgroup and alkyl chain are 0.28 and 0.21 nm^2, respectively,[55] there is sufficient space between ion-paired alkyl sulfates to accommodate the alkyl chains of additional surfactant. Furthermore, such an interdigitated monolayer configuration would yield a theoretical, total surface concentration of adsorbed surfactant of 4.5×10^{-10} mol cm^{-2}, which agrees reasonably well with our SPR results (i.e., $\Gamma = 3.9-4.4 \times 10^{-10}$ mol cm^{-2} for $C_{12}SO_4^-$) given the heterogeneous organization of $FcC_{12}SAu$ across the SAM and experimental uncertainty in the data.

It is noteworthy that adsorption of $NaC_{12}SO_4$ above the cmc to a cationic $^+(CH_3)_3N(CH_2)_{11}SAu$ SAM of charge density of +38 μC cm^{-2} and electrified single-crystal Au (111) surface at charge densities from +33 to +40 μC cm^{-2} yields adsorbed layer thicknesses of ∼2 nm and surface concentrations of $\sim 7-8 \times 10^{-10}$ mol cm^{-2}.[53,56] A continuous, liquid-crystalline bilayer morphology is proposed (Scheme 1C).[54,56] AFM imaging by Burgess et al. as a function of the voltage applied to the Au(111) electrode shows a transition from hemicylindrical micelle stripes at low metal charge densities (from −10 to +7 μC cm^{-2}) to a homogeneous phase at higher charge densities (from +33 to +40 μC cm^{-2}).[52,57] This morphological transition is accompanied by a doubling of the adsorbed surfactant concentration from 4×10^{-10} to 8×10^{-10} mol cm^{-2}.[53,57]

While oxidation of all of the available ferrocenes of the $FcC_{12}SAu$ SAM yields a theoretical ferrocenium charge density (+43 μC cm^{-2}) equivalent to that required to support a continuous bilayer of dodecyl sulfate, our SPR data is consistent with formation of a surface monolayer. We attribute the different adsorption morphology on $Fc^+C_{12}SAu$ SAMs to the following factors. First, the electrogenerated ferrocenium charge density of +23 ± 5 μC cm^{-2} is not sufficient to support an alkyl sulfate bilayer, whose formation requires at least +33 μC cm^{-2}.[53,57] Second, the $Fc^+C_{12}SAu$ SAM is not a fixed-charge surface like in the case of the $^+(CH_3)_3N(CH_2)_{11}SAu$ SAM, where the positive surface charge density is fixed in magnitude and position.[56] The concentration of surface-bound ferrocenium cations and their average spacing change continuously during the course of the anodic potential scan. Attempts to mimic a fixed-charge surface by instantaneously stepping the applied potential from open circuit (reduced SAM state) to +500 mV (oxidized SAM state) did not yield higher surface concentrations of $C_{12}SO_4^-$. Third, formation of discrete ferrocenium−alkyl sulfate ion pairs to stabilize the electrogenerated surface-bound cations is not driven by pure electrostatics (i.e., Coulomb attraction) as in the case of surfactant anion adsorption to the charged single-crystal Au(111) electrode and cationic SAM surfaces. The lateral mobility and redistribution of the surface charge at the Au(111) electrode during the linear potential scan enables the surface micelles ($\Gamma = 4 \times 10^{-10}$ mol cm^{-2}) formed at lower potentials and small metal charge densities, due to regulation of the charge position, to evolve into a homogeneous bilayer ($\Gamma = 8 \times 10^{-10}$ mol cm^{-2}) at more positive potentials and high positive charge densities via reorganization of the already adsorbed surfactant and adsorption of additional surfactant.[52−54,56,57] Since only one-half of the SAM-tethered ferrocenes are oxidized in the presence of alkyl sulfate, formation of a ferrocenium−alkyl sulfate ion pair does not facilitate subsequent oxidation of a neighboring ferrocene. Charge regulation does not appear to be operative during electrochemical oxidation of $FcC_{12}SAu$ SAMs in the presence of anionic surfactant.[56]

■ CONCLUSIONS

We investigated the redox electrochemistry of ferrocenyldodecanethiolate SAMs in aqueous solutions of surface-active sodium *n*-alkyl sulfates with chain lengths of 6−12 carbons at concentrations below, at, and above the critical micelle concentration. We demonstrated that the potential-induced ion pairing of the alkyl sulfates with SAM-bound ferroceniums leads to an unprecedented electrochemical behavior of the ferrocenylalkanethiolate SAM and interfacial aggregation of the amphiphilic anions at the SAM/aqueous solution interface.

While CVs acquired in $NaClO_4$ show two distinct ferrocene populations, single redox peaks are observed in the NaC_nSO_4 solutions. Approximately one-half of the available surface ferrocenes are reversibly oxidized in the presence of the alkyl sulfate anions in contrast to the total oxidation that occurs with the perchlorate anions. Oxidation and ion pairing with alkyl sulfate of roughly every second surface-tethered ferrocene preserves in the SAM oxidized state the attractive interactions that exist between clustered ferrocenylalkanethiolates in the reduced SAM, resulting in anodic peak full widths at half heights that are significantly less than 90.6 mV, in contrast to the broader anodic peaks and repulsive electrostatic interactions that dominate between neighboring perchlorate-paired ferroceniums. A longer alkyl chain increases the ability of the alkyl sulfate anion to pair with the SAM-bound ferrrocenium, akin to the greater ion-pairing capabilities of more hydrophobic inorganic anions versus hydrophilic ones, resulting in a lower apparent redox potential. A difference of six carbons in the hydrocarbon chain of the alkyl sulfate imparts a difference in ion-pairing ability (ion-pair formation constant) that is at least 100 times larger than that reported between some of the most hydrophilic and hydrophobic inorganic anions.

The SAM redox potential, anodic-to-cathodic peak separation, and full width at half-maximum of the anodic peak are sensitive to the surfactant aggregation state in solution. Plots of these parameters versus the logarithm of the molar concentration of NaC_nSO_4 show distinct breaks around the cmc. The non-Nernstian variation of the redox potential of the SAM-bound ferrocenes is related to the activity of the alkyl sulfate anion in the bulk solution. The presence of micelles in solution at surfactant concentrations > cmc results in decreased peak widths and separations. Acquisition of cyclic voltammograms as a function of the sodium alkyl sulfate concentration therefore provides a simple and rapid method to detect formation of micelles from dissociated anions.

dx.doi.org/10.1021/ja408512q | J. Am. Chem. Soc. 2013, 135, 17457−17468

The adsorbed surfactant anions adopt an interdigitated monolayer structure on the ferrocenium SAM that differs from the hemicylindrical micellar aggregates or bilayer film formed by electrostatic adsorption to charged surfaces. The ferrocenium SAM does not behave as a fixed-charge or charge-regulated surface (classic models) with respect to the potential-induced interfacial binding and organization of alkyl sulfates. We attribute this difference in behavior to steric crowding of the ferrocenes, which prevents the maximum ferrocenium charge density to be achieved, and the specific nature of the charge-transfer-induced ion-pairing interactions versus electrostatic forces.

■ ASSOCIATED CONTENT

Supporting Information

Additional results, examples of the mathematical deconvolution of the voltammetric peaks and determination of the ferrocenium charge density, plot of the log of the calculated ClO_4^- activity versus the log of the $NaClO_4$ concentration, and summary of the adsorbed dodecyl sulfate layer thicknesses and surface concentrations reported for different interfaces. This material is available free of charge via the Internet at http://pubs.acs.org.

■ AUTHOR INFORMATION

Corresponding Author

antonella.badia@umontreal.ca.

Present Address

[†]Department of Chemistry, McGill University, 801 Sherbrooke Street West, Montreal, QC H3A 2K6, Canada.

Notes

The authors declare no competing financial interest.

■ ACKNOWLEDGMENTS

This work was supported by grants to A.B. from the Natural Sciences and Engineering Research Council of Canada (NSERC), Canada Research Chairs Program, and Canada Foundation for Innovation. E.R.D. thanks Dr. Renaud Cornut for enlightening discussions.

■ REFERENCES

(1) Chidsey, C. E. D. *Science* **1991**, *251*, 919−922.
(2) Smalley, J. F.; Feldberg, S. W.; Chidsey, C. E. D.; Linford, M. R.; Newton, M. D.; Liu, Y.-P. *J. Phys. Chem.* **1995**, *99*, 13141−13149.
(3) Weber, K.; Hockett, L.; Creager, S. *J. Phys. Chem. B* **1997**, *101*, 8286−8291.
(4) Smalley, J. F.; Finklea, H. O.; Chidsey, C. E. D.; Linford, M. R.; Creager, S. E.; Ferraris, J. P.; Chalfant, K.; Zawodzinski, T.; Feldberg, S. W.; Newton, M. D. *J. Am. Chem. Soc.* **2003**, *125*, 2004−2013.
(5) Chidsey, C. E. D.; Bertozzi, C. R.; Putvinski, T. M.; Mujsce, A. M. *J. Am. Chem. Soc.* **1990**, *112*, 4301−4306.
(6) Collard, D. M.; Fox, M. A. *Langmuir* **1991**, *7*, 1192−1197.
(7) Rowe, G. K.; Creager, S. E. *Langmuir* **1991**, *7*, 2307−2312.
(8) Uosaki, K.; Sato, Y.; Kita, H. *Langmuir* **1991**, *7*, 1510−1514.
(9) Cruañes, M. T.; Drickamer, H. G.; Faulkner, L. R. *Langmuir* **1995**, *11*, 4089−4097.
(10) Finklea, H. O. Electrochemistry of Organized Monolayers of Thiols and Related Molecules on Electrodes. In *Electroanalytical Chemistry: A Series of Advances*; Bard, A. J., Rubinstein, I., Eds.; Marcel Dekker: New York, 1996; Vol. *19*, pp 109−335 and references therein.
(11) Ju, H.; Leech, D. *Phys. Chem. Chem. Phys.* **1999**, *1*, 1549−1554.
(12) Kondo, T.; Okamura, M.; Uosaki, K. *J. Organomet. Chem.* **2001**, *637−639*, 841−844.
(13) Auletta, T.; van Veggel, F. C. J. M.; Reinhoudt, D. N. *Langmuir* **2002**, *18*, 1288−1293.
(14) Valincius, G.; Niaura, G.; Kazakevičienė, B.; Talaikytė, Z.; Kažemėkaitė, M.; Butkus, E.; Razumas, V. *Langmuir* **2004**, *20*, 6631−6638.
(15) Lee, L. Y. S.; Sutherland, T. C.; Rucareanu, S.; Lennox, R. B. *Langmuir* **2006**, *22*, 4438−4444.
(16) Tian, H.; Dai, Y.; Shao, H.; Yu, H.-Z. *J. Phys. Chem. C* **2012**, *117*, 1006−1012.
(17) Rowe, G. K.; Creager, S. E. *J. Phys. Chem.* **1994**, *98*, 5500−5507.
(18) Norman, L. L.; Badia, A. *J. Phys. Chem. C* **2011**, *115*, 1985−1995.
(19) Creager, S. E.; Rowe, G. K. *Anal. Chim. Acta* **1991**, *246*, 233−239.
(20) Yokota, Y.; Yamada, T.; Kawai, M. *J. Phys. Chem. C* **2011**, *115*, 6775−6781.
(21) Rosen, M. J. *Surfactants and Interfacial Phenomena*, 3rd ed.; John Wiley and Sons, Inc.: Hoboken, NJ, 2004; pp 47−52.
(22) Norman, L. L.; Badia, A. *Langmuir* **2007**, *23*, 10198−10208.
(23) Evans, D. F.; Wennerström, H. *The Colloidal Domain Where Physics, Chemistry, Biology, and Technology Meet*: Wiley-VCH: New York, 1999; pp 168−170.
(24) Israelchvili, J. *Intermolecular and Surface Forces*, 2nd ed.; Academic Press: San Diego, CA, 1992.
(25) Kale, K. M.; Cussler, E. L.; Evans, D. F. *J. Solut. Chem.* **1982**, *11*, 581−592.
(26) Bhattacharyya, S. *J. Org. Chem.* **1998**, *63*, 7101−7102.
(27) Tazaki, M.; Okada, K.; Yakata, K.; Nakano, K.; Sakai, M.; Yonemitsu, T. *Phosphorus Sulfur* **2000**, *167*, 239−249.
(28) Bard, A. J.; Faulkner, L. R. *Electrochemical Methods Fundamentals and Applications*, 2nd ed.; J. Wiley & Sons: New York, 2001.
(29) Badia, A.; Chen, C.-I.; Norman, L. L. *Sens. Actuators, B: Chem.* **2013**, *176*, 736−745.
(30) Harvey, A. H.; Gallagher, J. S.; Sengers, J. M. H. L. *J. Phys. Chem. Ref. Data* **1998**, *27*, 761−774.
(31) De Feijter, J. A.; Benjamins, J.; Veer, F. A. *Biopolymers* **1978**, *17*, 1759−1772.
(32) Grassi, J. H.; Georgiadis, R. M. *Anal. Chem.* **1999**, *71*, 4392−4396.
(33) Jung, L. S.; Campbell, C. T.; Chinowsky, T. M.; Mar, M. N.; Yee, S. S. *Langmuir* **1998**, *14*, 5636−5648.
(34) Popenoe, D. D.; Deinhammer, R. S.; Porter, M. D. *Langmuir* **1992**, *8*, 2521−2530.
(35) Abbott, N. L.; Whitesides, G. M. *Langmuir* **1994**, *10*, 1493−1497.
(36) Rowe, G. K.; Creager, S. E. *Langmuir* **1994**, *10*, 1186−1192.
(37) Calvente, J. J.; Andreu, R.; Molero, M.; Lopez-Perez, G.; Domínguez, M. *J. Phys. Chem. B* **2001**, *105*, 9557−9568.
(38) Wandlowski, T.; Hromadova, M.; de Levie, R. *Langmuir* **1997**, *13*, 2766−2772.
(39) Hoeft, C. E.; Zollars, R. L. *J. Colloid Interface Sci.* **1996**, *177*, 171−178.
(40) Chen, K.; Schmittel, M. *Analyst* **2013**, *138*, 2405−2410.
(41) Skoog, D. A.; West, D. M.; Holler, F. J.; Crouch, S. R. *Fundamentals of Analytical Chemistry*; Brooks/Cole: Belmont, CA, 2004; pp 593−613.
(42) Kielland, J. *J. Am. Chem. Soc.* **1937**, *59*, 1675−1678.
(43) Cutler, S. G.; Meares, P.; Hall, D. G. *J. Chem. Soc., Faraday Trans. 1* **1978**, *74*, 1758−1767.
(44) Sasaki, T.; Hattori, M.; Sasaki, J.; Nukina, K. *Bull. Chem. Soc. Jpn.* **1975**, *48*, 1397−1403.
(45) Redepenning, J.; Tunison, H. M.; Finklea, H. O. *Langmuir* **1993**, *9*, 1404−1407.
(46) Williams, E. J.; Smolen, V. F. *J. Pharm. Sci.* **1972**, *61*, 639−641.
(47) Umeda, K.-i.; Fukui, K.-i. *Langmuir* **2010**, *26*, 9104−9110.
(48) Tajima, K. *Bull. Chem. Soc. Jpn.* **1971**, *44*, 1767−1771.
(49) Levchenko, A. A.; Argo, B. P.; Vidu, R.; Talroze, R. V.; Stroeve, P. *Langmuir* **2002**, *18*, 8464−8471.
(50) Martinez, J.; Talroze, R.; Watkins, E.; Majewski, J. P.; Stroeve, P. *J. Phys. Chem. C* **2007**, *111*, 9211−9220.
(51) Turner, S. F.; Clarke, S. M.; Rennie, A. R.; Thirtle, P. N.; Cooke, D. J.; Li, Z. X.; Thomas, R. K. *Langmuir* **1999**, *15*, 1017−1023.
(52) Burgess, I.; Jeffrey, C. A.; Cai, X.; Szymanski, G.; Galus, Z.; Lipkowski, J. *Langmuir* **1999**, *15*, 2607−2616.

(53) Burgess, I.; Zamlynny, V.; Szymanski, G.; Lipkowski, J.; Majewski, J.; Smith, G.; Satija, S.; Ivkov, R. *Langmuir* **2001**, *17*, 3355−3367.
(54) Leitch, J. J.; Collins, J.; Friedrich, A. K.; Stimming, U.; Dutcher, J. R.; Lipkowski, J. *Langmuir* **2012**, *28*, 2455−2464.
(55) Sigal, G. B.; Mrksich, M.; Whitesides, G. M. *Langmuir* **1997**, *13*, 2749−2755.
(56) Tulpar, A.; Ducker, W. A. *J. Phys. Chem. B* **2004**, *108*, 1667−1676.
(57) Chen, M.; Burgess, I.; Lipkowski, J. *Surf. Sci.* **2009**, *603*, 1878−1891.
(58) Gray, D. E. Section 6: Optics. In *American Institute of Physics Handbook*, 3rd ed.; McGraw-Hill: New York, 1972; pp 40−41.
(59) Palik, E. D. *Handbook of Optical Constants of Solids*; Academic Press, Inc.: Orlando, 1985.
(60) Ohtsuka, T.; Sato, K.; Uosaki, K. *Langmuir* **1994**, *10*, 3658−3662.